

**High-excitation and high-resolution photoluminescence spectra of bulk AlN**

Martin Feneberg,\* Robert A. R. Leute, Benjamin Neuschl, and Klaus Thonke  
*Institut für Quantenmaterie/Gruppe Halbleiterphysik, Universität Ulm, 89069 Ulm, Germany*

Matthias Bickermann

*Institut für Werkstoffwissenschaften 6, Universität Erlangen, 91058 Erlangen, Germany*

(Received 29 December 2009; revised manuscript received 26 May 2010; published 16 August 2010)

Photoluminescence spectra of high-quality bulk AlN crystals are reported. In addition to the expected linear luminescence features like free excitons and donor-bound excitons, nonlinear processes like biexcitons and the exciton-exciton scattering band are seen for higher excitation densities. For temperatures above  $\approx 150$  K the electron-hole plasma becomes clearly visible in the spectra. A detailed analysis of the data yields an exciton binding energy of 55 meV, a biexciton binding energy of 28.5 meV, a band gap of 6.089 eV at low temperature, and a band gap of 6.015 eV at room temperature.

DOI: [10.1103/PhysRevB.82.075208](https://doi.org/10.1103/PhysRevB.82.075208)

PACS number(s): 71.35.-y, 73.20.Mf

**I. INTRODUCTION**

Violet nitride-based laser diodes are a fully commercialized product for use in data storage systems, medical diagnostics, etc. While great improvements of such violet laser diodes can be expected to emerge as a result of intense research, many groups have shifted the development and research activities further into the blue/green spectral range or to the ultraviolet (UV) covered by AlGaIn/AlN.<sup>1</sup> Reports on electrically driven lasing in the far UV are rare<sup>2,3</sup> while optically pumped structures can be found more frequently.<sup>4,5</sup> Nevertheless, the basic physical processes involved in stimulated emission in AlGaIn,<sup>6</sup> and especially in AlN, are not yet completely clarified. In AlN, even the fundamental excitonic properties are not well established despite extensive research.<sup>7-12</sup> In this study, we investigate the luminescence properties of high-quality bulk AlN, especially under high-excitation density. To gain deeper insight into the high-excitation phenomena and to distinguish more clearly between different possible processes, we have performed temperature-dependent investigations. Presently, only few reports on optically pumped high-excitation recombination are available for AlN,<sup>13-15</sup> some of which have been performed exclusively at very low temperatures.<sup>14,15</sup> While in these studies biexciton luminescence as well as exciton-exciton scattering have been reported, no clear electron-hole plasma (EHP) was detected.

Here we report on biexcitons, exciton-exciton scattering, and EHP recombination, all observed in the same sample. The paper is organized as follows. After describing the experimental setup and sample properties, its linear optical response is described. In the following section, the high-excitation phenomena are analyzed and all of the observed phenomena are discussed in detail, resulting in exact values for the exciton binding energy as well as the biexciton binding energy. Finally, a summary is given.

**II. EXPERIMENTAL**

The sample was prepared from a high-quality bulk AlN crystal grown at temperatures exceeding 2000 °C by subli-

mation and recondensation of an AlN charge placed in a tungsten crucible.<sup>16,17</sup> A bulk AlN substrate was used as seed. Multiple resublimation of the source material prior to growth was employed in order to efficiently reduce the oxygen contamination. The sample was cut into a waferlike platelet and subsequently polished on both faces by standard techniques. The cut was performed in a way that the resulting surface normal is oriented approx. 45° off [0001]. The main part of the sample appears yellowish brown to the eye while some smaller regions appear colorless. Nevertheless, the 786- $\mu\text{m}$ -thick sample yields a flat optical transmittance exceeding 25% in the UV range of 3.3–5.6 eV (380–220 nm) across the whole area. This corresponds to absorption coefficients below 15  $\text{cm}^{-1}$ , indicating that the sample contains a fairly low concentration of deep level defects.<sup>17</sup> In mass spectrometry of companion samples, concentrations of oxygen, carbon, and silicon were determined to be  $4 \times 10^{18} \text{ cm}^{-3}$ ,  $2 \times 10^{18} \text{ cm}^{-3}$ , and  $7 \times 10^{17} \text{ cm}^{-3}$ , respectively.

Luminescence is excited by an ArF excimer laser ( $\lambda = 193 \text{ nm}$ , repetition rate 300 Hz) producing 4 ns long pulses with pulse energies ranging from  $E = 0.1$  to 3.5 mJ. For low-excitation photoluminescence (PL), the laser was operated at 0.1–0.2 mJ. High-excitation conditions were achieved by mounting an ultraviolet grade fused silica lens in the optical path and focusing the laser spot onto the sample. Variations in the excitation level were accomplished by changing the pulse energy. To account for nonlinear optical absorption in the optical components, we measured the laser power at the position of the sample. We estimate the excitation power on the sample surface to be between 5 and 60  $\text{MW}/\text{cm}^2$  for the focused laser.

For temperature-dependent experiments, the sample was placed in a liquid-helium cooled cryostat. The temperature was measured directly at the edge of the sample by a calibrated silicon diode. The emitted light was collected by a combination of a  $\text{MgF}_2$  coated parabolic aluminum mirror and an ultraviolet grade fused silica lens and directed to a monochromator with focal length of 1 m. Either a 1200 groove/mm or a 2400 groove/mm grating was used in first or second order, respectively. A cooled charge coupled device camera was mounted to the monochromator. The best spec-

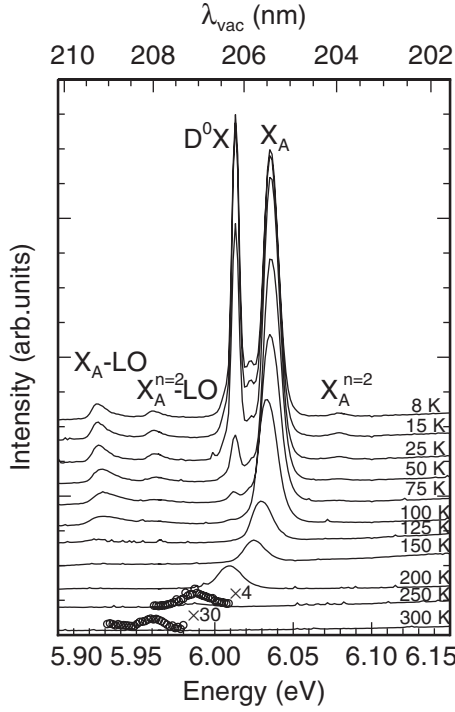


FIG. 1. Low-excitation PL spectra for increasing temperature. The assignments are  $X_A \rightarrow$  free exciton with a hole from the A valence band,  $X_A^{n=2} \rightarrow$  excited state of  $X_A$ ,  $D^0X \rightarrow$  donor bound exciton. LO  $\rightarrow$  longitudinal optical phonon replica of denoted band. For the 250 and 300 K spectra, the region of the peak is multiplied as indicated. Resolution was better than 5 meV at 6 eV here.

tral resolution used in this study was about  $3 \times 10^{-3}$  nm (better than 100  $\mu$ eV at 6 eV). Care was taken in calibration and we estimate our error to be in the range of the resolution limit.

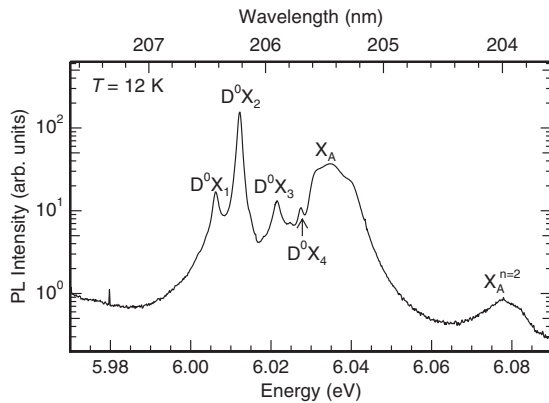


FIG. 2. Highly resolved free and bound exciton spectra (resolution better than 100  $\mu$ eV). The dominant donor-bound exciton line labeled ( $D^0, X_2$ ) at 6.012<sub>2</sub> eV has a FWHM of 1.4 meV after Gaussian fitting. The four clearly visible ( $D^0, X$ ) lines are enumerated from highest to lowest localization energy. These localization energies are 28.2 meV, 22.1 meV, 12.8 meV, and 7.2 meV, respectively, measured from the intensity maximum of the free-A exciton band.

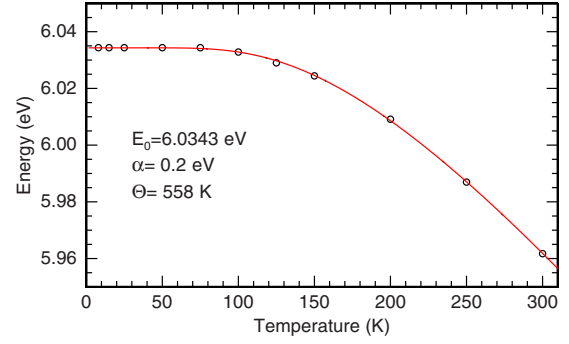


FIG. 3. (Color online) Temperature dependence of A free-exciton emission (symbols) and fit (line).

### III. RESULTS AND DISCUSSION

#### A. Free-excitonic recombination

In low-excitation PL, the free-exciton luminescence is easily identified by the typical increase in relative luminescence intensity for increasing temperature. It is clearly observable up to room temperature. Its low-temperature energy peak position is found to be 6.034<sub>3</sub> eV (from Figs. 1 and 2), shifting by as much as -74 meV for room temperature. The spectra are shown in Fig. 1.

Fitting the spectra for each temperature using Gaussian line shapes yields both the energy position of the free exciton and its intensity as a function of temperature. The temperature dependence of the energy is well described by the equation given by Viña *et al.*<sup>18</sup>

$$E(T) = E_0 - \frac{2\alpha}{\exp(\Theta/k_B T) - 1}, \quad (1)$$

where the parameters which describe the behavior best are  $E_0 = 6.034_3$  eV,  $\Theta = 558$  K, and  $\alpha = 0.2$  eV. This fit is shown in Fig. 3. These parameters are in very good agreement with our previous values for the temperature shift of AlN thin layers.<sup>19</sup> We also traced the temperature-dependent intensity of the free exciton to show its thermal quenching (Fig. 4). We find that the data are well reproduced by the simplest equation

$$I(T) = \frac{I_0}{1 + A \exp(-E_{act}/k_B T)}, \quad (2)$$

where the activation energy  $E_{act}$  is identical to the exciton binding energy. We wish to point out that this method provides less accuracy compared to analyzing the energy positions of excited states or the exciton-exciton scattering band when determining  $E_{bX}$ . However, the thermal quenching usually gives a lower limit of the true value. We find fitting parameters of  $A = 400$  and  $E_{act} = 47$  meV for Eq. (2). This value for the exciton binding energy is, within error margins, in agreement with the binding energy  $E_{bX}$  of  $(55 \pm 1)$  meV determined below in the context of the P band.

In the high-resolution spectra, the free-exciton emission shows a fine structure with three clearly separated distinct contributions. To unambiguously identify their origin, we performed polarized luminescence experiments. By tilting

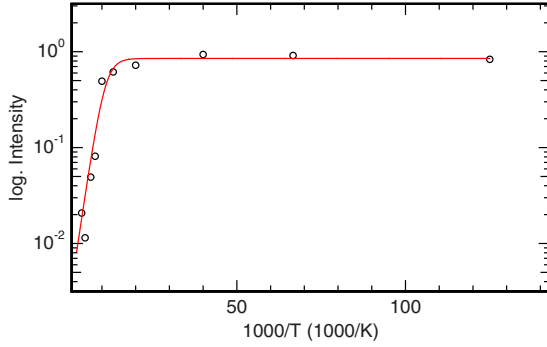


FIG. 4. (Color online) Temperature dependence of A free-exciton intensity (symbols) and fit (line).

the sample,  $\pi(E \parallel c, k \perp c)$  and  $\sigma(E \perp c, k \perp c)$  polarizations are accessible and comparable with our original unpolarized measurement (Fig. 5). We expect the transition from the  $\Gamma_7$  conduction band to the  $\Gamma_7$  (A) valence band to split into four states<sup>20</sup>

$$\Gamma_7 \times \Gamma_7 \rightarrow \Gamma_2 + \Gamma_1 + \Gamma_5(2). \quad (3)$$

The twofold-degenerate  $\Gamma_5$  states are split into longitudinal ( $\Gamma_{5L}$ ) and transverse ( $\Gamma_{5T}$ ) states for  $k \perp c$ . The  $\Gamma_{5T}$  is allowed for  $E \perp c$  only and forbidden for  $\parallel c$ . In principle, the  $\Gamma_1$  state is only allowed for  $E \parallel c$  polarization (with  $k \parallel c$ ). However, when the  $\Gamma_{5L}$  state mixes with  $\Gamma_1$  by  $k$ -linear terms for  $k \perp c$  both states ( $\Gamma_{5L}$  and  $\Gamma_1$ ) are allowed for both polarization directions. Finally, the  $\Gamma_2$  state is strictly forbidden for both polarization directions. Because  $|\Delta_{cr}| > |\Delta_{so}|$  in AlN we would expect the energetic order of these bands to be (from low to high energy):  $\Gamma_2, \Gamma_{5T}, \Gamma_{5L}, \Gamma_1$ .

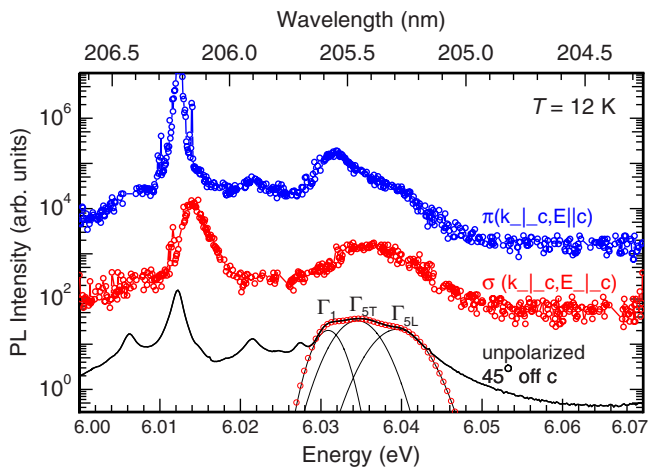


FIG. 5. (Color online) Polarized photoluminescence spectra of the free-exciton region together with the unpolarized measurement from the  $45^\circ$  off (0001) tilted sample (black continuous line).  $\pi$  polarization ( $k \perp c, E \parallel c$ ) is shown on top (blue) and  $\sigma$  polarization ( $k \perp c, E \perp c$ ) in the center (red). To the unpolarized measurement three Gaussian bands have been fitted in the energy region of the free A exciton to more exactly determine the energy positions. The sum of the fitted bands is plotted as red circles to show the quality of the fit.

Comparison of these predictions with our measurements allows a direct assignment of the peaks. Our experiments are shown in Fig. 5 together with a fit consisting of three Gaussian bands to accurately determine the peaks of the contributions. The  $\Gamma_1$  state, surprisingly, has the lowest energy and is located at 6.030<sub>9</sub> eV, visible in  $\pi$  polarization, whereas the  $\Gamma_5$  states are located at 6.034<sub>3</sub> eV ( $\Gamma_{5T}$ ) and 6.039<sub>3</sub> eV ( $\Gamma_{5L}$ ) and show up in  $\sigma$  polarization. Therefore the  $L$ - $T$  splitting energy in our AlN sample for the  $\Gamma_5$  states is  $\Delta_{L-T} = 5.0$  meV, close to the published value of 7.3 meV.<sup>21</sup> The discrepancy of the expected and observed order of  $\Gamma_1$  and  $\Gamma_5$  states can tentatively be explained by taking into account the polariton character of the states. The  $\Gamma_1$  state is probably visible for low  $k$  at lower energy where the character of its dispersion is mostly photonlike.

## B. Bound excitons

In addition to the free-exciton emission, donor-bound exciton recombinations ( $D^0, X$ ) are visible but already at  $T = 50$  K the free exciton is more intense. Highly resolved low-temperature spectra, shown in Fig. 2, allow us to distinguish between the different ( $D^0, X$ ) recombinations. The four clearly observable lines are located at 6.006<sub>1</sub>, 6.012<sub>2</sub>, 6.021<sub>5</sub>, and 6.027<sub>1</sub> eV while some fine structure is unresolved. The  $\Gamma_{5T}$  component of the free A exciton has its maximum at 6.034<sub>3</sub> eV, leading to localization energies of 28.2 meV, 22.1 meV, 12.8 meV, and 7.2 meV for the different ( $D^0, X$ ) lines, respectively. The dominant ( $D^0, X$ ) is the donor, with a localization energy  $E_{loc} = 22.1$  meV and a very low full width at half maximum (FWHM) of 1.4 meV, suggesting relatively low impurity concentrations and extremely low strain values. We believe that this donor is related to the chemical impurity silicon, having a donor binding energy of  $E_D = 250$  meV.<sup>22</sup> This assignment is in agreement with the available data for silicon in AlN, where  $E_{loc} = 24$  meV,<sup>23</sup>  $E_{loc} = 22-29$  meV,<sup>24</sup> and  $E_{loc} \approx 26$  meV (for the sample with the lowest Si doping in Ref. 25).

The other three lines are also tentatively ascribed to ( $D^0, X$ ) recombinations. For the line with  $E_{loc} = 7.2$  meV a ( $D^+, X$ ) assignment cannot be excluded. The ( $D^0, X$ ) having  $E_{loc} = 12.8$  meV is frequently dominating in high-quality epilayers<sup>15,26</sup> while sometimes in bulk material the dominant ( $D^0, X$ ) has  $E_{loc} = 30$  meV (Ref. 19) possibly identical to our ( $D^0, X$ ) having  $E_{loc} = 28.2$  meV.

## C. Identification of high-excitation bands

Recently, in AlN two different high-excitation effects were observed. A biexcitonic emission (M band) was found by Yamada *et al.*<sup>14</sup> at 19 meV and recently by our group at 27 meV below the free-exciton emission.<sup>15</sup> This value is directly the biexciton binding energy  $E_M$ . The discrepancy between these two values remains to be resolved.

Exciton-exciton scattering was also reported in Ref. 15. This so-called P band is expected to shift from higher to lower energies with increasing excitation density and helps in determining the exciton binding energy  $E_{bx}$ . A value of 48 meV was determined this way on thin epitaxial AlN layers.<sup>15</sup>

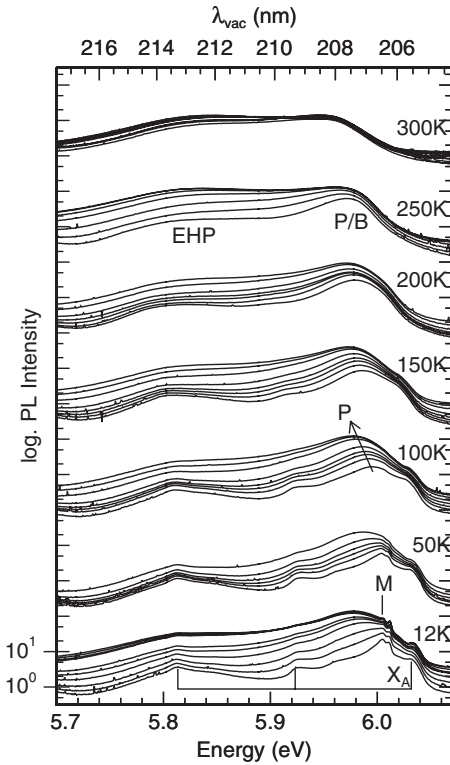


FIG. 6. Excitation power-dependent photoluminescence spectra from 5 to 60 MW/cm<sup>2</sup> at different temperatures from 12 K up to room temperature. For each temperature the logarithmic spectra are shifted vertically for better clarity. The assignments are  $X_A \rightarrow$  free exciton with a hole from the A-valence band, the first two LO phonon replica are indicated by the brackets,  $M \rightarrow$  biexciton,  $P \rightarrow$  exciton-exciton scattering band,  $B \rightarrow$  band-to-band recombination, and  $EHP \rightarrow$  electron-hole plasma.

High-excitation spectra, recorded at different temperatures from our sample, are summarized in Fig. 6. In addition to the linear excitonic recombinations, we observe additional bands at energies lower than the free and bound excitonic range. Luminescence related to the P band is visible in our spectra in Fig. 6 at around 5.98 eV as a broad featureless emission while we identify the relatively sharp and tiny feature at 6.004<sub>5</sub> eV as the M band or biexciton. It is only visible for the lowest temperatures.

At around 5.83 eV, an additional luminescence band arises with increasing temperature and excitation density. At 300 K and elevated pump densities this band dominates the spectra. It is assigned to the recombination of an EHP. As will be shown below, this band shows a behavior similar to the EHP in GaN, corroborating our interpretation.

One might argue that the exciton-electron scattering processes can lead to similar bands. Such a band arises from scattering of excitons with free electrons in the conduction band which have to be present in high density. In the case of our AlN sample, it is very unlikely to have such high concentrations of free electrons in the conduction band at room temperature. Taniyasu *et al.*<sup>22</sup> reported silicon to have a donor activation energy of 250 meV. Assuming a Boltzmann population, only about 1% would be activated at 300 K. We consider this amount to be negligible because our sample

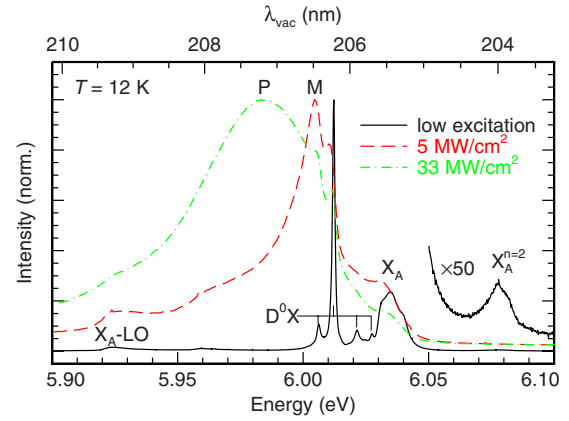


FIG. 7. (Color online) Comparison of low-excitation high-resolution photoluminescence (the resolution was better than 100  $\mu$ eV for this case) with two differently high-excited spectra at  $T=12$  K. The peaks are labeled as in Figs. 1 and 6.

does not show any electrical conductivity even for elevated temperatures ( $>300$  K).

For the following discussion of the behavior of the spectral features, all spectra shown in Fig. 6 have been fitted by three Gaussian bands, one accounting for the P band, one for the EHP, and an additional one at an energy position 20–45 meV below the P band. This additional band never becomes prominent, hampering the possibility to investigate its physical origin. It could be related to the broadening effects of both the P band and EHP band or replicas of dominant high-energy bands. Because we cannot assign it firmly, we do not add its intensity to any of the two other bands and omit it in our discussion for now.

Each band at each temperature and excitation density is analyzed in terms of peak position, intensity (area under the curve), and FWHM. It is worthwhile to mention that the fits agree extremely well with the measured spectra except for the low temperature and low-excitation intensity case. There, more sharp features are clearly visible, e.g., the biexciton or donor-bound exciton recombinations, hampering a simple fitting with only three bands. These features do not play any significant role when the excitation power is increased to 10 MW/cm<sup>2</sup> or above, or when the temperature is above 100 K.

#### D. Biexciton or M band

The biexciton recombination, also called excitonic molecule or M band, can be observed in our high-quality bulk sample in a temperature range up to 50 K. For the discussion we limit ourselves to this regime. In Fig. 7, a comparison of a low-excitation PL spectrum and two spectra recorded under different high-excitation levels is shown. All have been recorded at  $T=12$  K. The low-excitation PL shows clearly the free exciton with a hole of the A valence band centered at 6.034<sub>3</sub> eV. With increasing pump intensity, all spectral features show a shift of about 1.3 meV to lower energy, presumably due to heating of the sample through the intense laser pulses. Additionally, a new band arises at 6.004<sub>5</sub> eV, which we assign to the biexciton. Its binding energy, calculated as

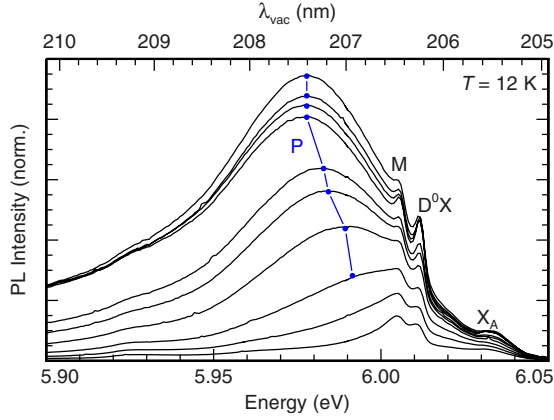


FIG. 8. (Color online) Photoluminescence spectra close to the band gap with increasing excitation density at  $T=12$  K. The excitation density is increased monotonously from bottom to top. The peaks are labeled as in Figs. 1 and 6. The shift of the P band is indicated by the blue signs.

the difference of the free-exciton energy to the biexciton recombination, is  $E_M=28.5$  meV, in agreement with our earlier report on heteroepitaxial layers.<sup>15</sup> When the excitation intensity is further increased, the P band becomes visible as the dominant band, having its maximum at 5.983 eV for 33 MW/cm<sup>2</sup> excitation intensity. However, the biexciton remains visible as a shoulder at 6.004<sub>5</sub> eV.

At temperatures above 50 K, the biexciton is barely visible due to the broadening of the nearby intense P band. In principal we expect biexcitons to be stable up to room temperature and above due to their high binding energy.

### E. Exciton-exciton scattering processes or the P bands

Exciton-exciton scattering processes occur when, at high enough exciton densities, inelastic collisions of excitons occur. One exciton is scattered into a higher excited state while the other one decays with equal-energy loss. As more scattering partners become available, the higher the probability that an exciton is not only scattered into its  $n=2$  state but that even scattering to  $n=3\cdots\infty$  is possible. The number  $n$  is usually given as an index to distinguish the different scattering events, therefore leading to  $P_2$  to  $P_\infty$  bands. In a simple hydrogenlike model, higher excited excitonic states are separated from the ground state by  $\Delta E_n=(1-1/n^2)E_{bX}$ . This means the first possible P band ( $P_2$ ) is located three quarters of the exciton binding energy below the free exciton while the last P band ( $P_\infty$ ) is separated by  $E_{bX}$ , when excitons are scattered into the continuum. We find a shift of the P band from higher to lower peak energy for increasing excitation power, as can be seen for the 12 K spectra in Fig. 8 in agreement with the model presented. Analysis of the peak positions is shown in Fig. 9, where indeed a shift from 41.7 meV at lower pumping to a limiting value of 55.3 meV at higher pumping is observable.

The latter number is the exciton binding energy in our sample. We also find excellent agreement with the value calculated from the  $P_2$  band by

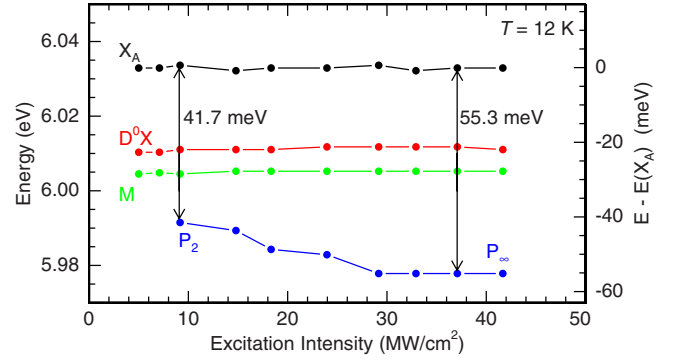


FIG. 9. (Color online) Peak positions of the different luminescence bands at  $T=12$  K as a function of the excitation intensity.

$$E_{bX} = \frac{4}{3} \Delta E(P_2) = \frac{4}{3} 41.7 \text{ meV} = 55.6 \text{ meV}. \quad (4)$$

The same calculation scheme can be used for the difference of the peak energies between  $P_2$  and  $P_\infty$  bands yielding  $E_{bX}=54.4$  meV. The free exciton with  $n=2$  is also observable directly at the high-energy side of the free exciton (Fig. 7) at 6.077 eV. Again, the energy to the free exciton ( $\Gamma_{5T}$ ) equals three quarters of  $E_{bX}$ , yielding  $E_{bX}=56.9$  meV. All four routes to determine  $E_{bX}$  yield very similar results, which we summarize as  $E_{bX}=(55 \pm 1)$  meV for the free  $X_A$  exciton.

This value compares well with our value determined by the thermal dissociation energy of the free exciton of 47 meV (see above) and recently published values ranging from 48,<sup>15,27</sup> 51,<sup>26</sup> up to 74 meV.<sup>28</sup> Still the range of reported values is comparably broad, leading to the natural assumption that the strain situation in the samples may influence  $E_{bX}$ , as discussed in Ref. 29.

In the effective-mass approximation, the above donor silicon induces a hydrogenlike state with binding energy

$$E_D = \frac{m_e R_y}{m_0 \epsilon^2}. \quad (5)$$

Here  $R_y=13.6$  eV is the Rydberg constant and  $m_0$  the free-electron mass. For the dielectric constant we use  $\epsilon=7.87$ .<sup>29</sup> By using  $E_D=250$  meV we get a value for the effective electron mass of  $m_e=1.1m_0$ . This value is considerably higher than the expected value of about  $m_e=0.3m_0$  (Ref. 30) leading to the conclusion that the effective-mass theory is not well suited to describe the silicon donor in AlN.

However, the free excitons are expected to follow more closely the effective-mass model. We use an effective electron mass of  $m_e=0.3m_0$  (Ref. 30) to estimate the effective hole mass in AlN. The exciton binding energy is given by

$$E_{bX} = \frac{R_y}{m_0 \epsilon^2} \left( \frac{1}{m_e} + \frac{1}{m_h} \right)^{-1}. \quad (6)$$

This results in an effective hole mass of  $m_h=1.5m_0$  for the highest valence band.

The intensity of the P band increases superlinearly with excitation power, having an exponent  $k$  of around 1.5 in this sample for both 12 and 50 K (Fig. 10), slightly lower than the value of  $k=1.6$  reported by Yamada *et al.*<sup>14</sup> and Leute *et*

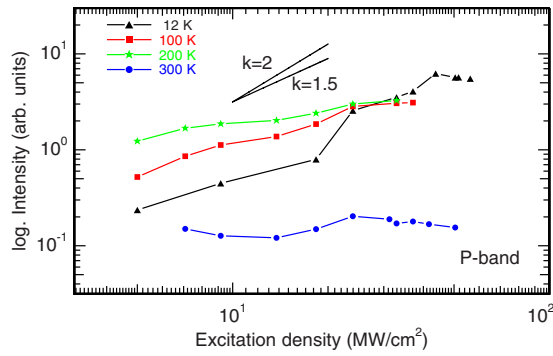


FIG. 10. (Color online) Integrated intensity of the P band (fitting results) as a function of temperature and excitation density. For comparison two lines with slope  $k=2$  and  $k=1.5$  are shown in the same graph.

*al.*<sup>15</sup> It is often discussed in the literature<sup>31,32</sup> that exponents below the ideal  $k=2$  are due to nonradiative recombination channels. In any case, we do observe the competing EHP process and biexcitonic recombination lowering the P-band recombination rate. When the temperature increases, the slope of this superlinear increase lowers successively. For  $T$  above 200 K the increase in the P band with increasing excitation density vanishes while the band still remains clearly distinguishable in the spectra (Fig. 10).

It is very interesting to observe the P-band intensity as a function of temperature while maintaining the excitation density. This represents a vertical cut through the data points of Fig. 10. An example for 24 MW/cm<sup>2</sup> is shown in Fig. 11. It can be clearly seen that the absolute intensity of the P band increases from 12 to 200 K, decreasing then again for higher temperatures. This behavior has been observed in GaN (Ref. 33) and it was suggested that the threshold of high-excitation emission bands is different for different temperatures.<sup>34</sup> In GaN, the EHP emission has a lower threshold than the P band for temperatures higher than 200 K, in qualitative agreement with our findings for AlN.

At high temperatures and high excitation we observe a decreasing energy spacing to the free-exciton energy. This indicates that at elevated temperatures the P band is con-

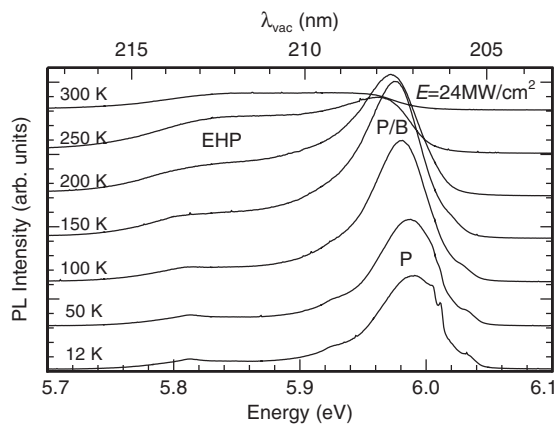


FIG. 11. Temperature dependence of high-excitation spectra with constant excitation density of 24 MW/cm<sup>2</sup>. The peaks are labeled as in Fig. 6.

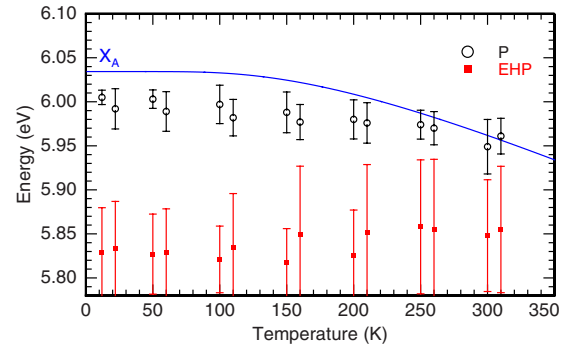


FIG. 12. (Color online) Energy positions of high-excitation bands (fitting results) as a function of sample temperature in comparison with the free-exciton energy position. Shown are data points for 5 and 24 MW/cm<sup>2</sup>, the latter being shifted laterally by +10 K for better visibility. The full width of half maximum of the bands is indicated by error bars.

verted into a merged band possibly consisting of inelastic exciton scattering and band-to-band recombination. This band is usually called the B band. Unfortunately, we are not able to determine the exact conditions where the P band transforms into the B band but the following arguments may give a hint: for  $T > 200$  K the distance of P-band peak and free-exciton position at low-excitation level is about 25 meV while the FWHM of the P band is 50 meV (Fig. 12). It is reasonable that the merged band occurs at least for higher temperatures and/or pump power densities. This means the P band slightly changes its character with increasing temperature without any sharp transition. As already mentioned, the superlinear increase in the P band is also no longer detectable at  $T > 200$  K. This might be the signature of the dominating B-band contribution.

## F. EHP

The band at about 5.83 eV at 12 K in our measurements (Fig. 6) is assigned to the recombination of an electron-hole plasma. Similarities to EHP recombination in GaN are obvious.<sup>33</sup> We observe a strong band-gap renormalization for these high-excitation densities. However, when increasing the excitation density further, the band does not shift to lower energies as expected.

In Fig. 12, the positions of P band and EHP peak positions are shown as a function of temperature for two different excitation densities. The free-exciton recombination position is also shown as a solid line. Obviously, the distance between EHP peak and free-exciton emission decreases slightly when increasing the pump power for temperatures below 200 K. Only for 250 and 300 K a small downshift is observed: the energy spacing between the EHP and free-exciton position increases with increasing excitation density. To complicate the case further, the peak emission of the observed EHP emission decreases the energy spacing to the free-exciton emission as a function of temperature as well.

To explain this complex behavior satisfactorily we have to assume the temperature of the carriers inside the EHP as being different from that of the lattice. For increasing plasma

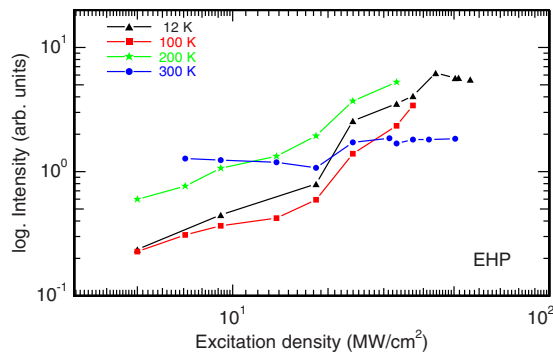


FIG. 13. (Color online) Integrated intensity of the EHP (fitting results) as a function of temperature and excitation density in same absolute units as Fig. 10.

temperatures in GaN, an absolute blueshift of the EHP peak emission was reported.<sup>35</sup> The physical explanation of this effect is the increased kinetic energy of the carriers inside the plasma, shifting the peak to higher energies. In our spectra, the plasma temperature cannot be easily deduced by fitting the high-energy slope of the EHP because other luminescence bands are overlapping. Therefore, we assume the plasma temperature depends on the FWHM of the EHP emission, which is fitted by a Gaussian line shape. The FWHM of the EHP is shown in Fig. 12 by error bars. It is seen that the FWHM increases for increasing excitation density and temperature and therefore does the plasma temperature. At 250 and 300 K this broadening seems to saturate. We assign this to the activation of competing nonradiative recombination channels with short decay time, effectively reducing our plasma density.<sup>35</sup> One possibility for such a channel would be, e.g., Auger recombination. The EHP emission unambiguously, up to  $T=250$  K, shows a superlinear increase for increasing excitation density (Fig. 13), corroborating our explanation.

For our crude estimation of the average carrier density within the electron-hole plasma, we compare our data with an experimental report on GaN.<sup>36</sup> There, the EHP is located about 100–200 meV below the band gap for carrier densities between  $1.6 \times 10^{19}$  and  $1.1 \times 10^{20}$  cm<sup>-3</sup>. We take into account that the energy renormalization due to high carrier densities is material independent in units of the exciton binding energy.<sup>32,37</sup> The exciton binding energies of GaN and

AlN are about 25 meV (Ref. 38) and 55 meV, respectively. Therefore, the renormalization energies for similar carrier densities can be transferred from GaN to AlN by simply multiplying by a factor of  $55/25=2.2$ . For our observed  $\Delta E=200$  meV at 12 K (Fig. 12), we obtain a carrier density within the EHP slightly below  $10^{19}$  cm<sup>-3</sup>, which is a reasonable value.

#### IV. SUMMARY

In conclusion, we investigated high-excitation photoluminescence in bulk AlN. Three different mechanisms were identified: biexcitonic decay, exciton-exciton scattering (P band), and EHP recombination. The biexciton binding energy was determined to be 28.5 meV. From the P band, we consistently evaluated the exciton binding energy to be  $(55 \pm 1)$  meV in this sample. This value is in agreement with the thermal activation of the free exciton and its energy spacing from the  $n=2$  excited state. At higher temperatures, the P band merges with band-to-band recombination while under the same conditions the EHP arises. The EHP does not shift to lower energies for increasing excitation densities and is explained by competing nonradiative recombination channels which are subsequently activated by increasing the lattice temperature and the plasma temperature through intense excitation. The EHP is the dominant recombination process for high-excitation densities at room temperature. As a by-product of our investigation, we find consistent values for the band-gap energies of nominally unstrained bulk AlN: at room temperature (300 K) we find  $E_g=6.015$  eV while at 12 K this value equals 6.089 eV for the transition from the conduction band to the highest valence band. The effective hole mass of this valence band is estimated to be  $m_h=1.5m_0$ .

#### ACKNOWLEDGMENTS

We thank Tobias Meisch (Institut für Quantenmaterie, Universität Ulm, Germany) for help with the polarized luminescence measurements, Anna V. Rodina (A.F. Ioffe Physico-Technical Institute, St. Petersburg, Russia) for valuable discussions, and Chris L. Littler (Department of Physics, North Texas State University, USA) for critical reading the manuscript.

\*Present address: Institut für Experimentelle Physik, Otto-von-Guericke-Universität Magdeburg, Magdeburg, Germany; martin.feneberg@ovgu.de

<sup>1</sup>Y. Taniyasu, M. Kasu, and T. Makimoto, *Nature (London)* **441**, 325 (2006).

<sup>2</sup>H. Yoshida, Y. Yamashita, M. Kuwabara, and H. Kan, *Appl. Phys. Lett.* **93**, 241106 (2008).

<sup>3</sup>H. Yoshida, Y. Yamashita, M. Kuwabara, and H. Kan, *Nat. Photonics* **2**, 551 (2008).

<sup>4</sup>T. Takano, Y. Narita, A. Horiuchi, and H. Kawanashi, *Appl.*

*Phys. Lett.* **84**, 3567 (2004).

<sup>5</sup>M. Kneissl, Z. Yang, M. Teepe, C. Knollenberg, O. Schmidt, P. Kiesel, N. M. Johnson, S. Shujman, and L. J. Schowalter, *J. Appl. Phys.* **101**, 123103 (2007).

<sup>6</sup>S. Bidnyk, J. B. Lam, B. D. Little, Y. H. Kwon, J. J. Song, G. E. Bulman, H. S. Kong, and T. J. Schmidt, *Appl. Phys. Lett.* **75**, 3905 (1999).

<sup>7</sup>J. Li, K. B. Nam, M. L. Nakarmi, J. Y. Lin, and H. X. Jiang, *Appl. Phys. Lett.* **81**, 3365 (2002).

<sup>8</sup>J. Li, K. B. Nam, M. L. Nakarmi, J. Y. Lin, H. X. Jiang, P.

- Carrier, and S.-H. Wei, *Appl. Phys. Lett.* **83**, 5163 (2003).
- <sup>9</sup>T. Onuma, S. F. Chichibu, T. Sota, K. Asai, S. Sumiya, T. Shibata, and M. Tanaka, *Appl. Phys. Lett.* **81**, 652 (2002).
- <sup>10</sup>E. Silveira, J. A. Freitas, M. Kneissl, D. W. Treat, N. M. Johnson, G. A. Slack, and L. J. Schowalter, *Appl. Phys. Lett.* **84**, 3501 (2004).
- <sup>11</sup>E. Silveira, J. A. Freitas, O. J. Glembocki, G. A. Slack, and L. J. Schowalter, *Phys. Rev. B* **71**, 041201 (2005).
- <sup>12</sup>L. Chen, B. J. Skromme, R. F. Dalmau, R. Schlessler, Z. Sitar, C. Chen, W. Sun, J. Yang, and M. A. Khan, *Appl. Phys. Lett.* **85**, 4334 (2004).
- <sup>13</sup>E. Kuokstis, J. Zhang, Q. Fareed, J. W. Yang, G. Simin, M. A. Khan, R. Gaska, M. Shur, J. C. Rojo, and L. J. Schowalter, *Appl. Phys. Lett.* **81**, 2755 (2002).
- <sup>14</sup>Y. Yamada, K. Choi, S. Shin, H. Murotani, T. Taguchi, N. Okada, and H. Amano, *Appl. Phys. Lett.* **92**, 131912 (2008).
- <sup>15</sup>R. A. R. Leute, M. Feneberg, R. Sauer, K. Thonke, S. B. Thapa, F. Scholz, Y. Taniyasu, and M. Kasu, *Appl. Phys. Lett.* **95**, 031903 (2009).
- <sup>16</sup>B. Epelbaum, M. Bickermann, and A. Winnacker, *J. Cryst. Growth* **275**, e479 (2005).
- <sup>17</sup>M. Bickermann, B. M. Epelbaum, O. Filip, P. Heimann, S. Nagata, and A. Winnacker, *Phys. Status Solidi C* **7**, 21 (2010).
- <sup>18</sup>L. Viña, S. Logothetidis, and M. Cardona, *Phys. Rev. B* **30**, 1979 (1984).
- <sup>19</sup>G. M. Prinz, A. Ladenburger, M. Feneberg, M. Schirra, S. B. Thapa, M. Bickermann, B. M. Epelbaum, F. Scholz, K. Thonke, and R. Sauer, *Superlattices Microstruct.* **40**, 513 (2006).
- <sup>20</sup>P. P. Paskov, T. Paskova, P. O. Holtz, and B. Monemar, *Phys. Rev. B* **64**, 115201 (2001).
- <sup>21</sup>H. Murotani, T. Kuronaka, Y. Yamada, T. Taguchi, N. Okada, and H. Amano, *J. Appl. Phys.* **105**, 083533 (2009).
- <sup>22</sup>Y. Taniyasu, M. Kasu, and T. Makimoto, *Appl. Phys. Lett.* **85**, 4672 (2004).
- <sup>23</sup>G. M. Prinz, A. Ladenburger, M. Schirra, M. Feneberg, K. Thonke, R. Sauer, Y. Taniyasu, M. Kasu, and T. Makimoto, *J. Appl. Phys.* **101**, 023511 (2007).
- <sup>24</sup>G. M. Prinz, M. Feneberg, M. Schirra, R. Sauer, K. Thonke, S. B. Thapa, and F. Scholz, *Phys. Status Solidi (RRL)* **2**, 215 (2008).
- <sup>25</sup>K. B. Nam, M. L. Nakarmi, J. Li, J. Y. Lin, and H. X. Jiang, *Appl. Phys. Lett.* **83**, 2787 (2003).
- <sup>26</sup>T. Onuma, T. Shibata, K. Kosaka, K. Asai, S. Sumiya, M. Tanaka, T. Sota, A. Uedono, and S. F. Chichibu, *J. Appl. Phys.* **105**, 023529 (2009).
- <sup>27</sup>T. Koyama, M. Sugawara, T. Hoshi, A. Uedono, J. F. Kaeding, R. Sharma, S. Nakamura, and S. F. Chichibu, *Appl. Phys. Lett.* **90**, 241914 (2007).
- <sup>28</sup>A. Sedhain, N. Nepal, M. L. Nakarmi, T. M. Al tahtamouni, J. Y. Lin, H. X. Jiang, Z. Gu, and J. H. Edgar, *Appl. Phys. Lett.* **93**, 041905 (2008).
- <sup>29</sup>H. Ikeda, T. Okamura, K. Matsukawa, T. Sota, M. Sugawara, T. Hoshi, P. Cantu, R. Sharma, J. F. Kaeding, S. Keller, U. K. Mishra, K. Kosada, K. Asai, S. Sumiya, T. Shibata, M. Tanaka, J. S. Speck, S. P. DenBaars, S. Nakamura, T. Koyama, T. Onuma, and S. Chichibu, *J. Appl. Phys.* **102**, 123707 (2007).
- <sup>30</sup>I. Vurgaftman and J. R. Meyer, *J. Appl. Phys.* **94**, 3675 (2003).
- <sup>31</sup>A. Yamamoto, K. Miyajima, T. Goto, H. J. Ko, and T. Yao, *J. Appl. Phys.* **90**, 4973 (2001).
- <sup>32</sup>T. J. Inagaki and M. Aihara, *Phys. Rev. B* **65**, 205204 (2002).
- <sup>33</sup>J.-C. Holst, L. Eckey, A. Hoffmann, I. Broser, H. Amano, and I. Akasaki, *MRS Internet J. Nitride Semicond. Res.* **2**, 25 (1997).
- <sup>34</sup>S. Bidnyk, T. J. Schmid, B. D. Little, and J. J. Song, *Appl. Phys. Lett.* **74**, 1 (1999).
- <sup>35</sup>S. Juršėnas, G. Kurilčik, G. Tamulaitis, A. Žukauskas, R. Gaska, M. S. Shur, M. A. Khan, and J. W. Wang, *Appl. Phys. Lett.* **76**, 2388 (2000).
- <sup>36</sup>T. Nagai, T. J. Inagaki, and Y. Kanemitsu, *Appl. Phys. Lett.* **84**, 1284 (2004).
- <sup>37</sup>P. Vashishta and R. K. Kalia, *Phys. Rev. B* **25**, 6492 (1982).
- <sup>38</sup>K. Kornitzer, T. Ebner, K. Thonke, R. Sauer, C. Kirchner, V. Schwegler, M. Kamp, M. Leszczynski, I. Grzegory, and S. Porowski, *Phys. Rev. B* **60**, 1471 (1999).